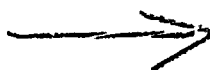


AD P00529

EJECTOR NOZZLE DEVELOPMENT



by

E. J. Schum and J. H. DeHart

Rockwell International, North American Aircraft Division

ABSTRACT

A combination of computer analysis and scale model testing was utilized to develop a nozzle which would increase the performance of thrust augmenting ejectors. Scale model tests were conducted on various multi-lobed and vortex generating nozzles. Predicted jet characteristics were obtained by calculating a finite difference solution of Reynolds equations for the three dimensional flow field. A two-equation turbulence kinetic energy model was used for closure. It is demonstrated that the thrust augmentation of the XFV-12A ejector can be increased from 1.45 to 1.64 by the addition of lobes to the baseline nozzle, and a corresponding increase of throat width.

INTRODUCTION

The static thrust of turbojet engines can be significantly increased by diverting the exhaust flow through an ejector pump. According to the laws of momentum and energy conservation, greatest thrust is obtained from a given energy input by accelerating a large mass of air to a low exhaust velocity. Within an ejector, thrust is increased by transferring the kinetic energy of the engine exhaust stream to a larger mass of air drawn from the atmosphere. The ejector duct experiences a reaction force which is equal but opposite to the momentum change of the accelerated stream. Details of this process have been discussed by Bevilaqua.¹

The mechanism of this energy transfer is the turbulent mixing of the two streams. Thus, increases in ejector thrust augmentation can be obtained by increasing the turbulent mixing rate. Appreciable increases in mixing and augmentation have been achieved with the so-called hypermixing^{2,3}. The alternating exit of the hypermixing nozzle serves to introduce a row of streamwise vortices into a plane jet (Figure 1).

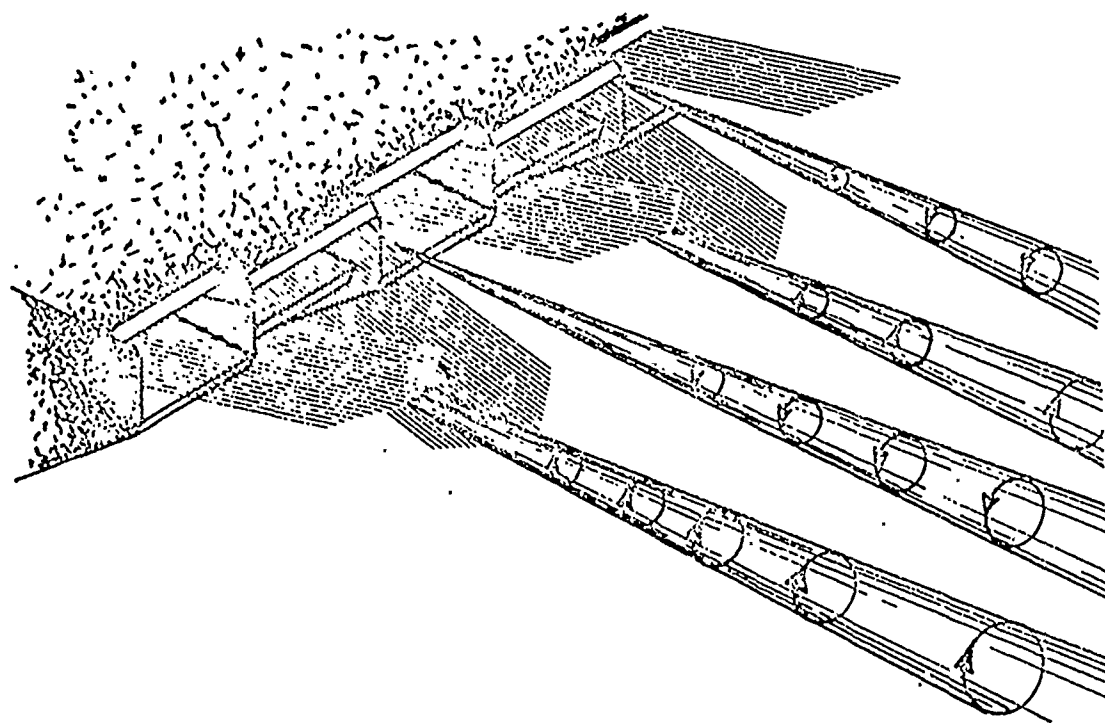


Figure 1. Hypermixing Nozzle Exit

These vortices serve to accelerate the turbulent mixing and thus to entrain additional fluid into the ejector. Because of their favorable entrainment characteristics, hypermixing nozzles in the centerbody were used in the XFV-12A airplane. Figure 2 illustrates how the ejector components fold into the shape of a wing for forward flight. This study is concerned with the development of the centerbody nozzle.

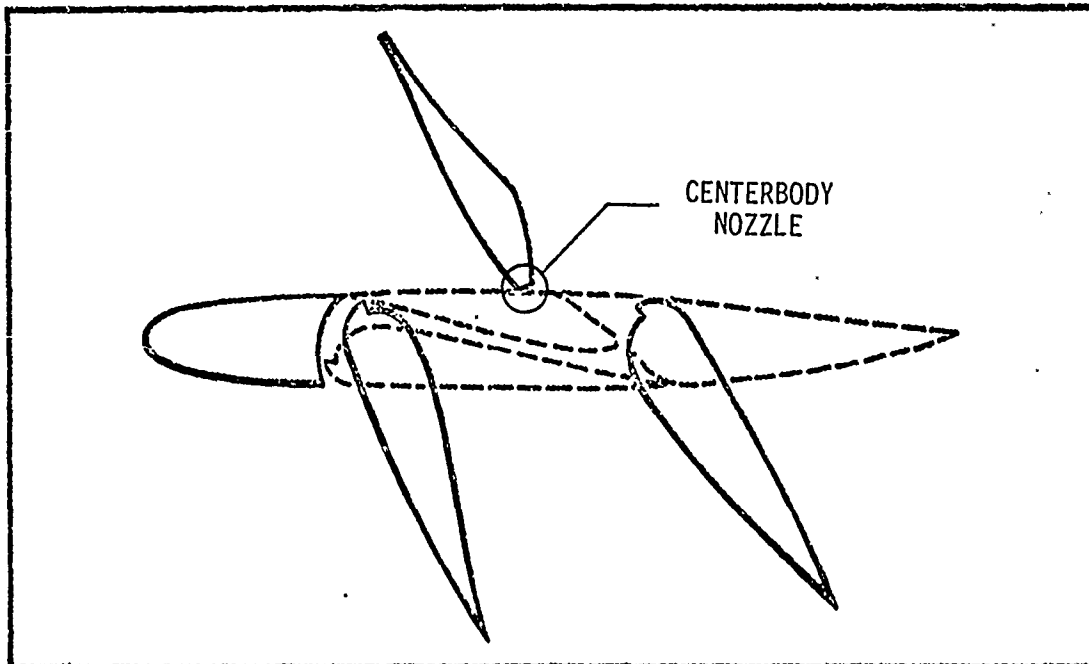


Figure 2. Deflected Ejector wing

The specific objective of this investigation was to develop and demonstrate centerbody nozzles that would provide increased augmentation, exceeding the peak value of 1.45 obtained for the hypermix configuration.

In the following sections, a "master plan" is presented including a brief description of the 3-dimensional, turbulent kinetic energy program (3D-TKE) used to calculate the viscous mixing. Analytical and experimental results for both symmetric and asymmetric, centerbody nozzle configurations are discussed.

NOZZLE DEVELOPMENT PLAN

The overall program consisted of three phases.

Phase I To Improve Analytical Capability for Calculating 3-Dimensional, Turbulent Flow by:

- Identifying inlet turbulent kinetic properties for augmenters (k, μ_t, ϵ)
- Inlet grid generation program
- Simplification for incompressible flow

Phase II To Compare Analyses with Experiment for Hypermixing Nozzles to Update Analytical Technique

Phase III To Develop and Demonstrate Centerbody Nozzles that Increase Augmentation

ANALYTICAL MODEL AND NUMERICAL APPROACH

Governing Equations

The program equations, in cartesian coordinates, include:

Equation of State

$$\rho = \frac{\bar{p}}{RT}$$

Continuity

$$\frac{\partial}{\partial X} (\rho U) + \frac{\partial}{\partial Y} (\rho V) + \frac{\partial}{\partial Z} (\rho W) = 0$$

Momentum

(1)

$$\frac{\partial}{\partial X} (\rho U^2) + \frac{\partial}{\partial Y} (\rho UV) + \frac{\partial}{\partial Z} (\rho UW) = \frac{\partial \tau_{YX}}{\partial Y} + \frac{\partial \tau_{ZX}}{\partial Z} - \frac{\partial \bar{p}}{\partial X}$$

$$\frac{\partial}{\partial X} (\rho UV) + \frac{\partial}{\partial Y} (\rho V^2) + \frac{\partial}{\partial Z} (\rho VW) = \frac{\partial \tau_{YY}}{\partial Y} + \frac{\partial \tau_{ZY}}{\partial Z} - \frac{\partial \bar{p}}{\partial Y}$$

$$\frac{\partial}{\partial X} (\rho UW) + \frac{\partial}{\partial Y} (\rho VW) + \frac{\partial}{\partial Z} (\rho W^2) = \frac{\partial \tau_{YZ}}{\partial Y} + \frac{\partial \tau_{ZZ}}{\partial Z} - \frac{\partial \bar{p}}{\partial Z}$$

Energy

$$\frac{\partial}{\partial X} (\rho UH) + \frac{\partial}{\partial Y} (\rho VH) + \frac{\partial}{\partial Z} (\rho WH) = \frac{\partial}{\partial Y} \left(\frac{\mu_t}{Pr} \frac{\partial H}{\partial Y} \right) + \frac{\partial}{\partial Z} \left(\frac{\mu_t}{Pr} \frac{\partial H}{\partial Z} \right)$$

where U, V, and W are the time averaged components. These equations are regarded as parabolic in the longitudinal coordinate, X, and elliptic in the transverse coordinates; Y and Z. A more complete description of the program is given by DeJooode and Patankar⁴.

The turbulent shear stresses, τ_{ij} , are expressed in terms of a turbulent viscosity, μ_t , and velocity gradients. The two-equation turbulence model of Launder and Spalding⁵ expresses the turbulent viscosity in terms of two parameters, K and ϵ , for which two differential equations are solved. The expression for μ_t is:

$$\mu_t = c_\mu \rho K^2 / \epsilon \quad (2)$$

where c_μ is an empirical constant and K and ϵ are obtained from the solution of:

$$\begin{aligned} \frac{\partial(\rho UK)}{\partial X} + \frac{\partial(\rho VK)}{\partial Y} + \frac{\partial(\rho WK)}{\partial Z} &= \frac{\partial}{\partial Y} \left(\frac{\mu_t}{\sigma_K} \frac{\partial K}{\partial Y} \right) + \frac{\partial}{\partial Z} \left(\frac{\mu_t}{\sigma_K} \frac{\partial K}{\partial Z} \right) + G - \rho \epsilon \\ \frac{\partial(\rho U\epsilon)}{\partial X} + \frac{\partial(\rho V\epsilon)}{\partial Y} + \frac{\partial(\rho W\epsilon)}{\partial Z} &= \frac{\partial}{\partial Y} \left(\frac{\mu_t}{\sigma_\epsilon} \frac{\partial \epsilon}{\partial Y} \right) \\ &+ \frac{\partial}{\partial Z} \left(\frac{\mu_t}{\sigma_\epsilon} \frac{\partial \epsilon}{\partial Z} \right) + (c_1 G - c_2 \rho \epsilon) \left(\frac{\epsilon}{K} \right) \end{aligned} \quad (3)$$

G is the rate of generation of K by the action of velocity gradients. Since the only significant gradients are $\partial U / \partial Y$ and $\partial U / \partial Z$, the expression for G becomes

$$G = \mu_t \left[\left(\frac{\partial U}{\partial Y} \right)^2 + \left(\frac{\partial U}{\partial Z} \right)^2 \right] \quad (4)$$

Values of the constants (Reference 5) include:

c_μ	c_1	c_2	σ_K	σ_ϵ
0.09	1.44	1.92	1.0	1.3

The above equations were put in finite difference form. From known conditions at an upstream cross section, X , the flow field at the downstream cross section, $X + \Delta X$ is computed. This streamwise marching process is continued until the domain of interest has been covered.

Boundary Conditions

Figure 3 presents a typical ejector configuration, containing a hypermix centerbody nozzle. Other types of centerbody nozzle designs can also be analyzed. Needed geometric parameters include the throat to inlet primary flow area, A_2/A_0 , the ejector exit to throat area, A_3/A_2 , the diffuser length, L , the Coanda surface shape, and the flow split or division of the primary flow between the centerbody nozzle and Coanda jets.

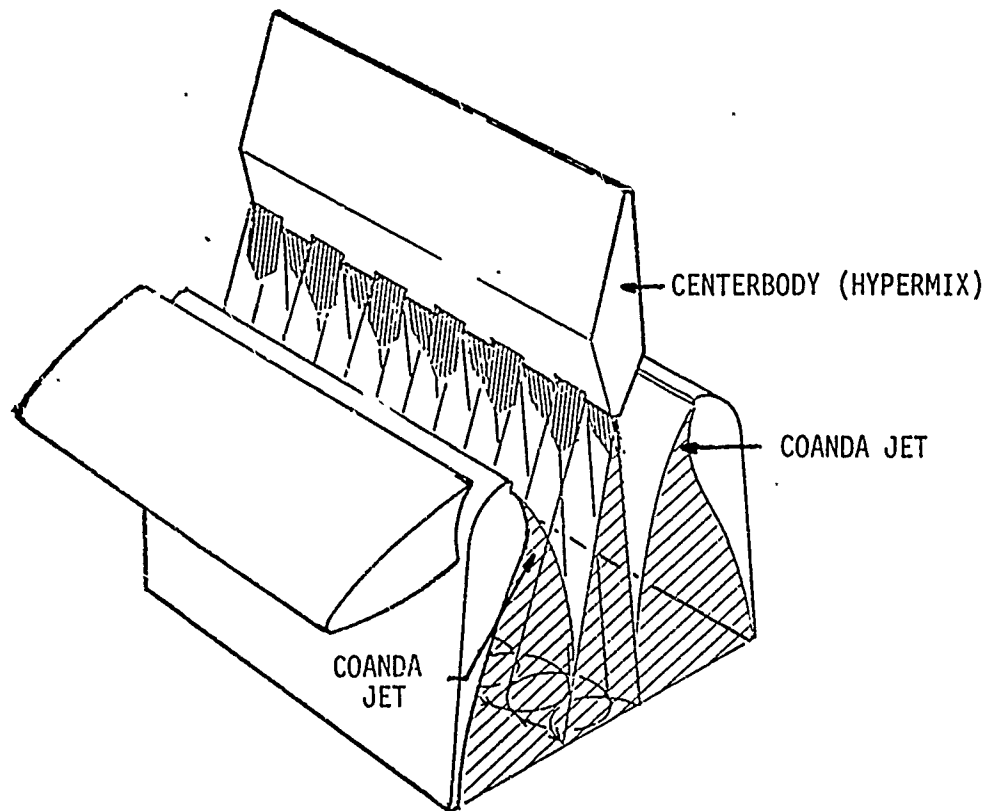


Figure 3. Typical Ejector Wing Configuration

The computational boundaries are outlined in Figure 4 for the hypermix type configuration. Symmetry planes are used as computational boundaries in the spanwise direction because most nozzle designs are "periodic" along the span.

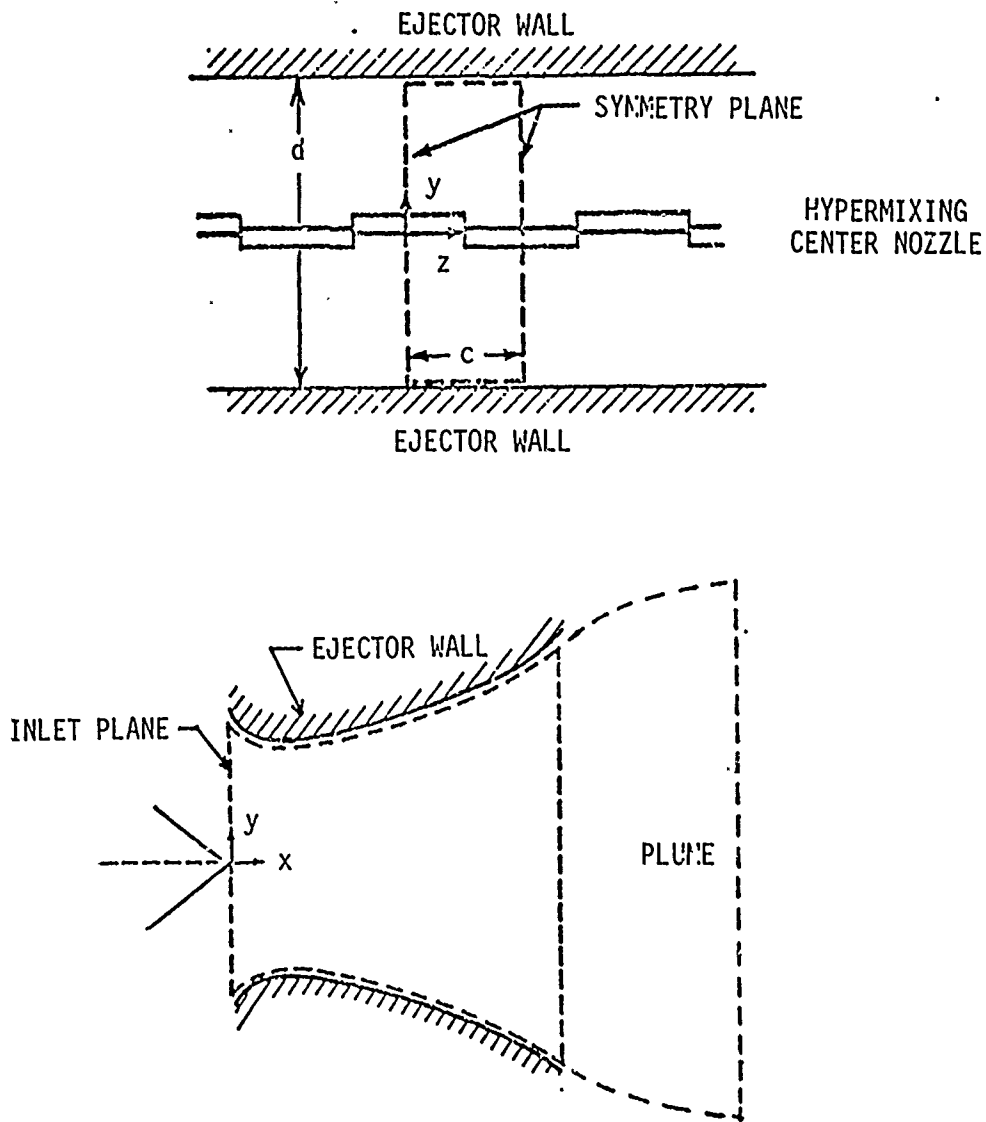


Figure 4. Computational Boundaries

Initial Conditions

Primary jet velocities were calculated from the conventional isentropic relation using a velocity coefficient of 0.925 (reference 6). The mean static pressure along with the ambient pressures are used in Bernoulli's equation to calculate the inlet secondary stream velocities. The inlet static pressure is obtained in the iterative solution of the viscous flow field and is discussed in the "Closure Scheme". Values of the initial turbulence conditions (K , μ_t , ϵ) are discussed in a later section.

Inlet Grid Generator

At the inlet computational plane of the ejector, it is necessary that the flow area be subdivided into a grid of approximately 1500 to 3000 control areas (volumes) with corresponding velocities (primary or secondary). To reduce the usual 20 hour setup time to an hour or less and also eliminate the arbitrariness of the subdivision, a computer program was written to generate the grid where only the ejector and nozzle dimensions are the primary input. A grid for the hypermix configuration is shown in Figure 5 and contains approximately 3000 control volumes. At the upper and lower surfaces, the grid appears to be shaded because in the Coanda jet region, a much finer grid is used.

Closure Scheme

Closure is obtained by iterating on the inlet pressure until the calculated pressure at the end of the exhaust plume is ambient. The plume exit pressure is dependent upon the curvature of the jet sheet leaving the trailing edge of the ejector shroud as well as the plume length, both determined by the difference between the ambient pressure and the ejector exit pressure. This "jet flap" effect is discussed in more detail in reference 4.

The thrust augmentation ratio, ϕ , is defined to be the ratio of the ejector stream thrust to the isentropic thrust obtained by expanding the same mass of primary fluid to atmospheric pressure. The thrust of the ejector is evaluated by integrating the exit momentum flux and pressure force,

$$T = \int_{A_3} \rho U^2 dY dZ - (P_\infty - P_3)A_3$$

in which P_3 and A_3 are the static pressure and area at the exit. ϕ is defined as:

$$\phi = \frac{T}{\dot{m}_{pri} U_{isent}}$$

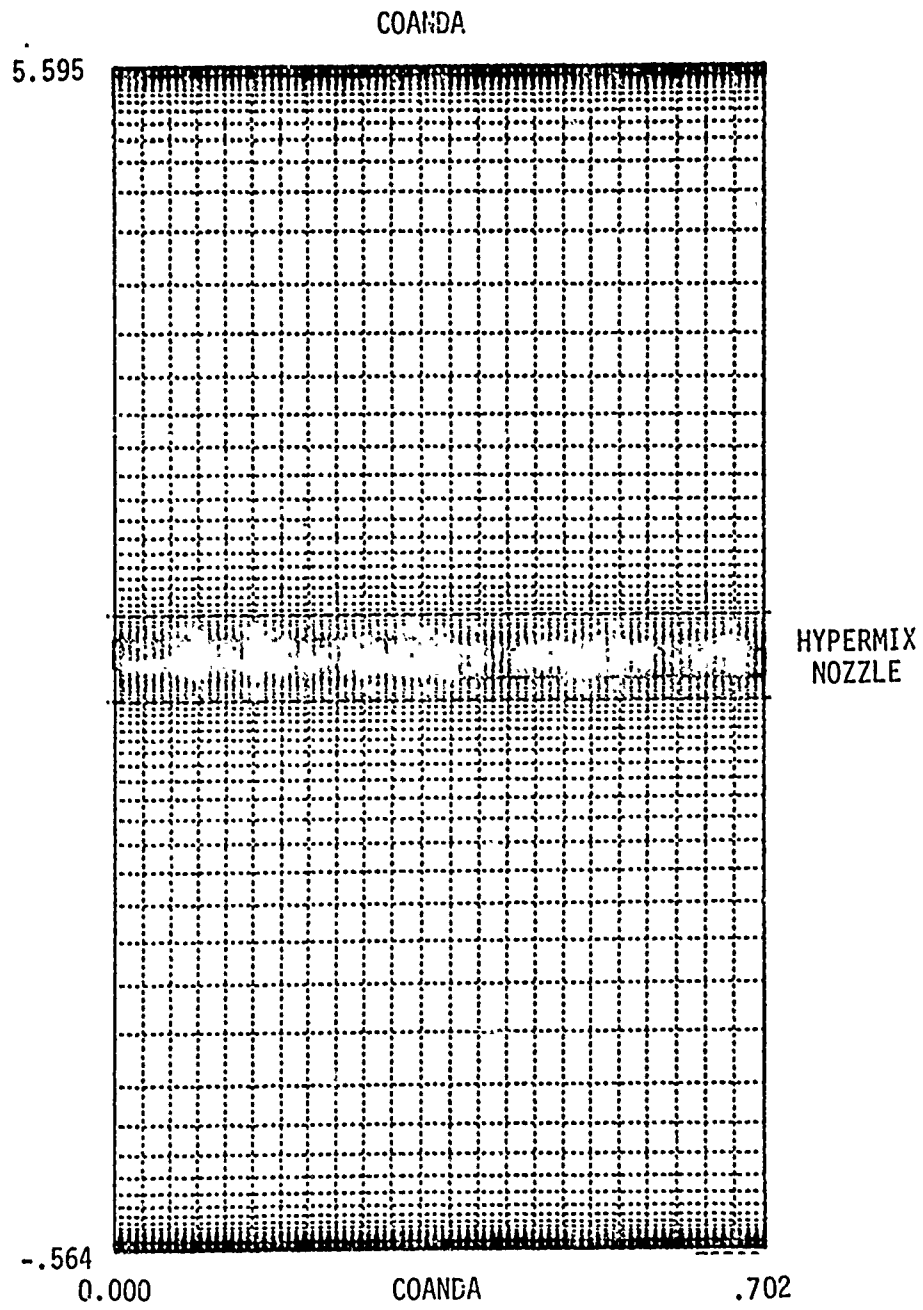


Figure 5. Computational Grid for Hypermixing Centerbody Configuration.

Simplification for Incompressible Flow

To reduce computer time the analysis was conducted using the incompressible option in the program. With this, density is assumed constant and the state and energy equations are bypassed. To verify that this was a valid approach, both compressible and incompressible computer runs were made for a hypermix configuration at a pressure ratio of 2.2 and primary gas temperatures of 80°F (usual test conditions). There was little difference in the ejector calculated exit velocity profiles. This afforded a saving of about 30 percent or 10 minutes of CPU time on the CDC-176 computer.

RESULTS AND DISCUSSION

The following sections describe how the hypermix test results interacted with the computer program development (Phase II) so that it could be used to identify higher performance symmetric and/or asymmetric nozzle configurations (Phase III).

Hypermixing Nozzles

To improve the analytical design methods, angularity measurements were made of the secondary flow at the ejector inlet. These data were generalized and incorporated into the program. Initial values of the kinetic energy for use at the inlet computational plane were obtained from hot film measurements.

Figure 6 presents the calculated, 2-dimensional mainstream velocity distribution along with the calculated and measured profiles for two lateral positions, corresponding to the middle of the hypermix element and between adjacent elements. It should be noted that the Coanda velocities are not in good agreement since Coanda curvature effects have not been included in the computer program. In the 2-dimensional velocity distribution, the nearby Coanda velocities were purposely omitted from the plot in order that the intermediate velocity distribution could be shown.

Calculated ϕ 's are compared with measured values in Figure 7. Analytical results were normalized at a ϕ of 1.45 at 7° since the computer program predicts a $\Delta\phi$. The 7° reference point corresponds to the ϕ measured for the 7° hypermixing nozzle configuration, used in the XFV-12A airplane. Results are for an $A_3/A_2 = 1.9$, $A_2/A_0 = 16.2$, and an $L/D = 1.8$, where D is the throat width. Up to about 20°, the predicted trend agrees with measured values. Beyond 20°, calculated ϕ 's decreased while the measured values remained essentially constant.

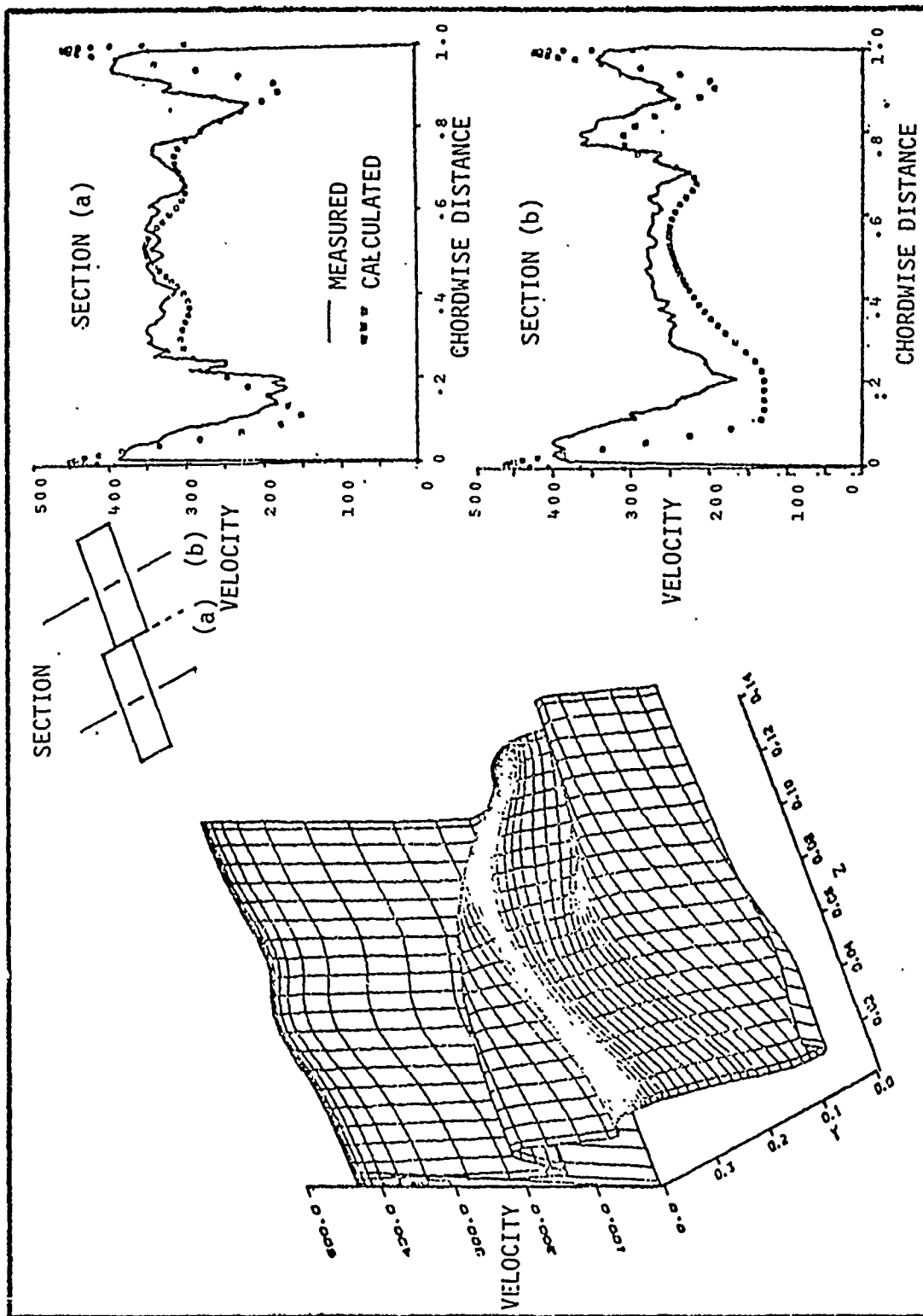


Figure 6. Comparison of Calculated and Measured Velocity Profiles at Ejector Exit for 22.5° Hypermix Nozzles

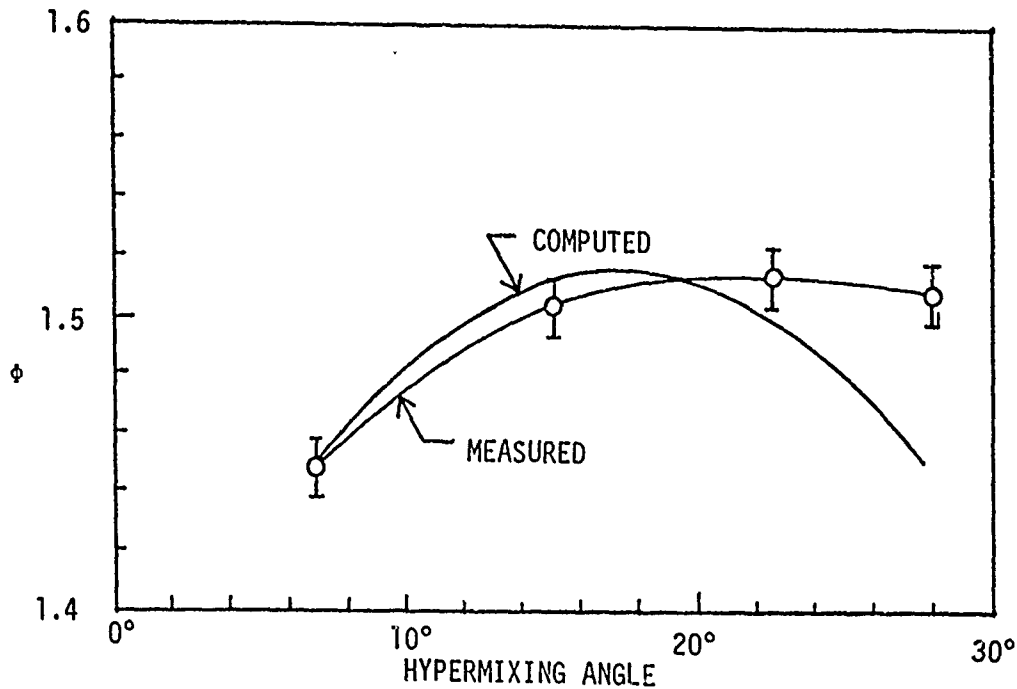


Figure 7. Comparison of Measured and Computed Augmentation

With the increasing hypermixing angle, the swirling or vortex action should increase and therefore additional swirl terms (originally deleted to reduce computer time) should be included in the turbulence generation term, G (Equation 4). With the addition of all swirl terms in G for the 28° case, the calculated ϕ increased by only 0.01. The lack of agreement beyond about 20° is attributed to a limitation in the manner used to solve the flow equations, in that the V and W velocity components should be much smaller than the mainstream velocity, U . At high swirl angles this may not be true.

Since good agreement of calculated and measured velocities were obtained along with the general ϕ trends, the computer program was used in the design and analyses of other nozzle configurations, discussed in the following sections.

Asymmetric Nozzles

This type nozzle was developed in an effort to capitalize on the generally superior entrainment characteristics of the symmetric cross-slot nozzle configuration while maintaining packaging limits imposed by supersonic airfoil contours. The design combines a series of aft facing, spanwise slot nozzles with an alternating series of cross-slots on the

forward side. An upstream view of the 14 element, asymmetric centerbody nozzle along with a side view is shown in Figure 8. The aspect ratio of the span slot is 5.5.

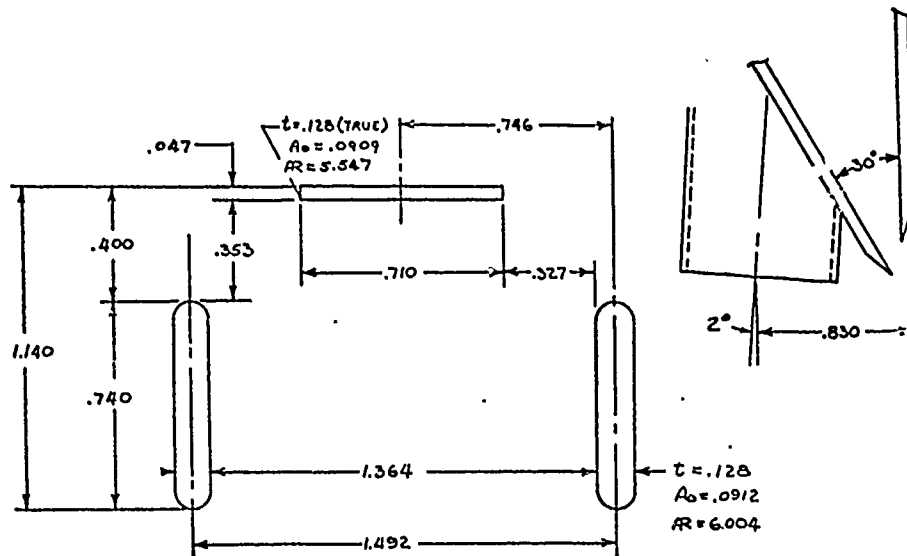


Figure 8. 14 Element Asymmetric Nozzle

The computer program was used to indicate expected $\Delta\phi$ trends. Tests were then used to confirm the predicted trends. For example, to increase ϕ it was analytically shown that for this type nozzle, it is necessary to increase the throat width, A_2 , to prevent the merging of the cross-slot and Coanda jets. In Figure 9 the measured maximum ϕ for the 5.4 aspect ratio configuration, wide throat was 1.53, an increase of 0.02 over the hypermixing peak value (Figure 7).

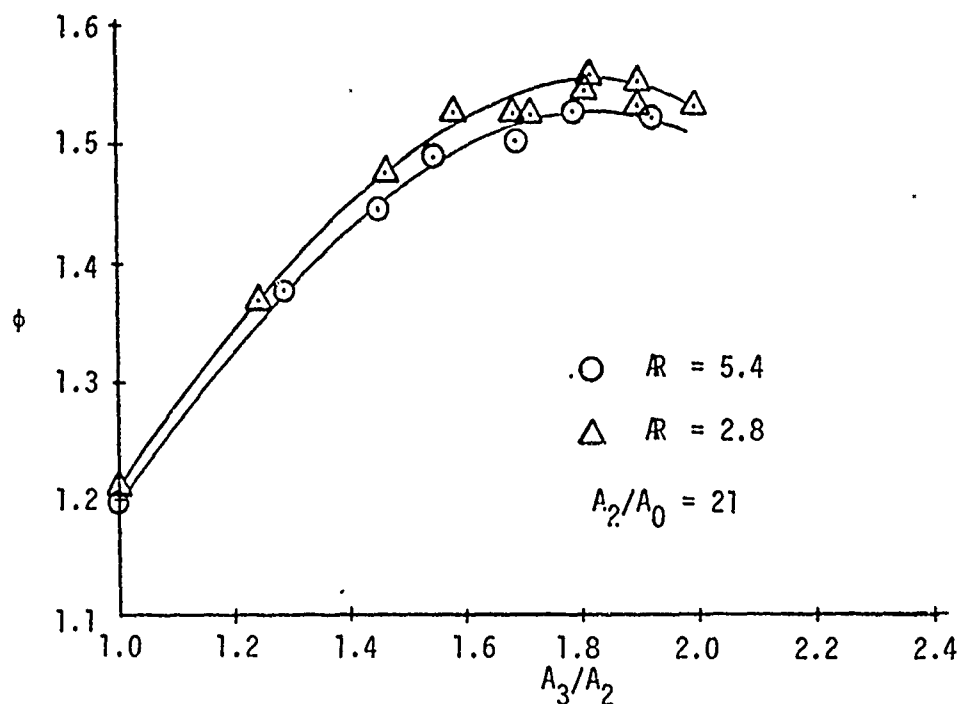


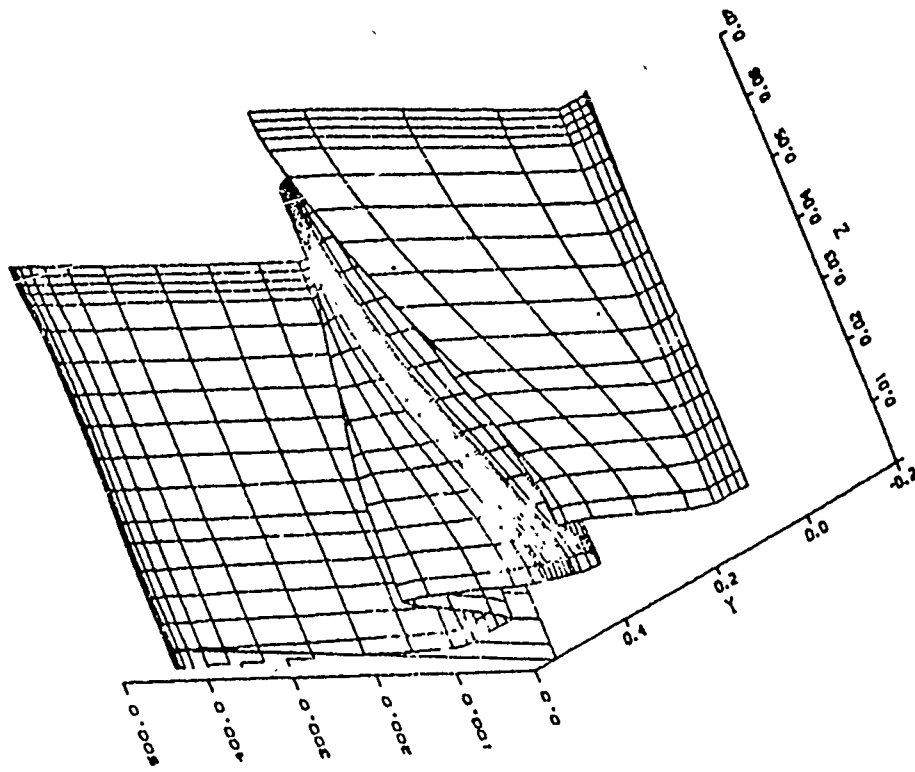
Figure 9. Effect of Span Slot Aspect Ratio, Asymmetric Nozzles

Further analyses showed that when the aspect ratio of the span slot is reduced from 5.5 to 2.8, the ϕ should increase by 0.03. Measurements (Figure 9) showed a gain of 0.02. The peak ϕ for the asymmetric configuration was 1.55, a $\Delta\phi$ of 0.04 above the peak for the hypermixing nozzles.

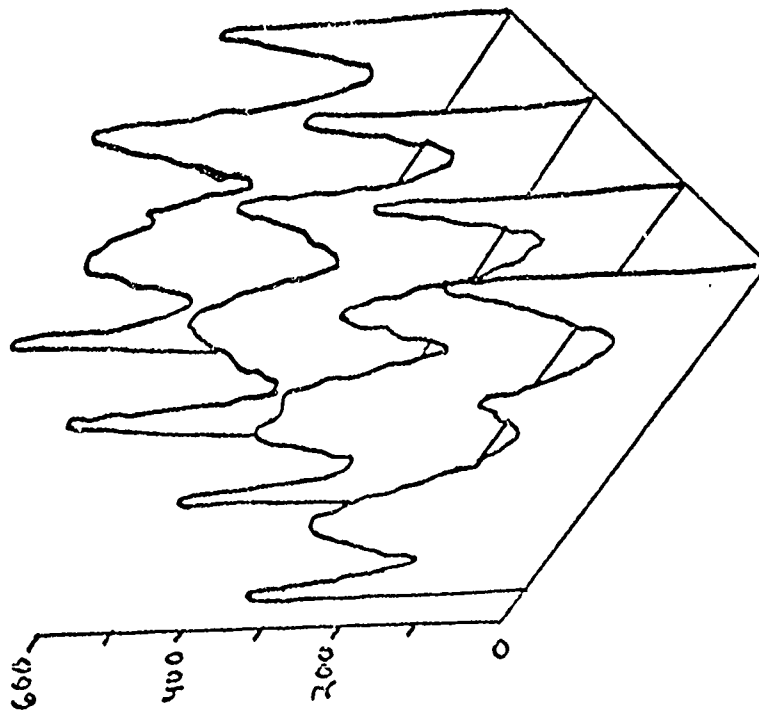
Calculated and measured velocities for the smaller aspect ratio configuration are shown in Figure 10. Velocity profiles are similar.

Symmetric Nozzles

Based on the previous analytical and experimental results neither the hypermixing or asymmetric nozzles provided a ϕ of the order of 1.65, the target value. The computer program, however, has been proven useful in their design and evaluation. To obtain reliable results, the program does require an accurate description of the flow conditions at the inlet computational plane, particularly that of the primary flow. Secondary flow angularity was discussed earlier. Therefore, the study of the symmetric nozzles was concerned with primary flow angularity measurements, the design and testing of a nozzle to capitalize on these measurements, and finally the effect of geometric variations on ϕ .



COMPUTED



MEASURED

Figure 10. Comparison of Velocity Profiles at Ejector Exit for Asymmetric Nozzles

The symmetric nozzle configurations consist of either a series of symmetric cross slots or a series of cross slots with intermediate span slots. Figure 11 shows schematically the downstream vortex action for symmetric cross slots, in the absence of span slots.

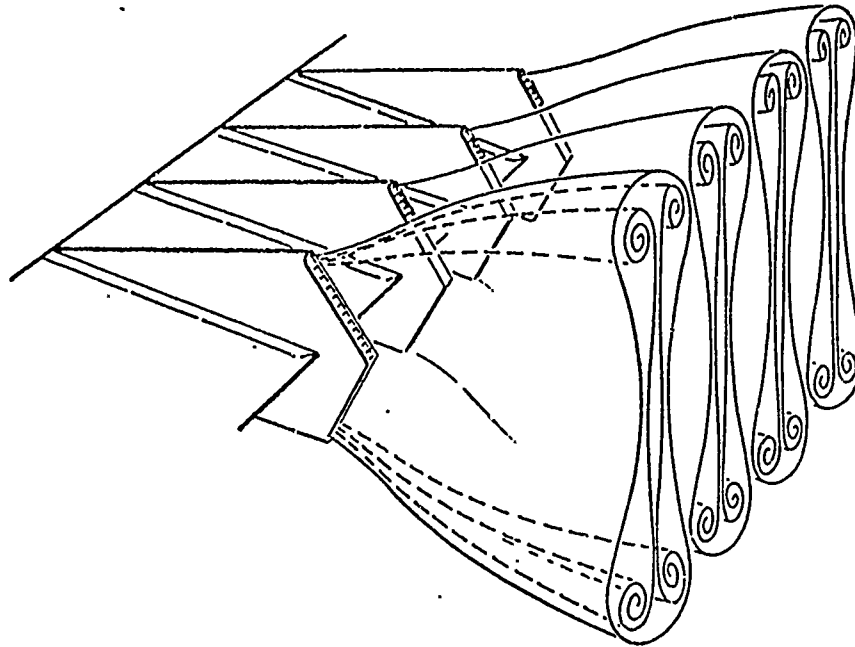


Figure 11. Symmetric Cross Slot Flow Pattern

Figure 12 presents a typical cross slot-span slot configuration. In this configuration the thickness of the cross slot gap is shown to vary linearly from the centerline. In other configurations this thickness is held constant. Geometric design parameters are shown in Figure 13.

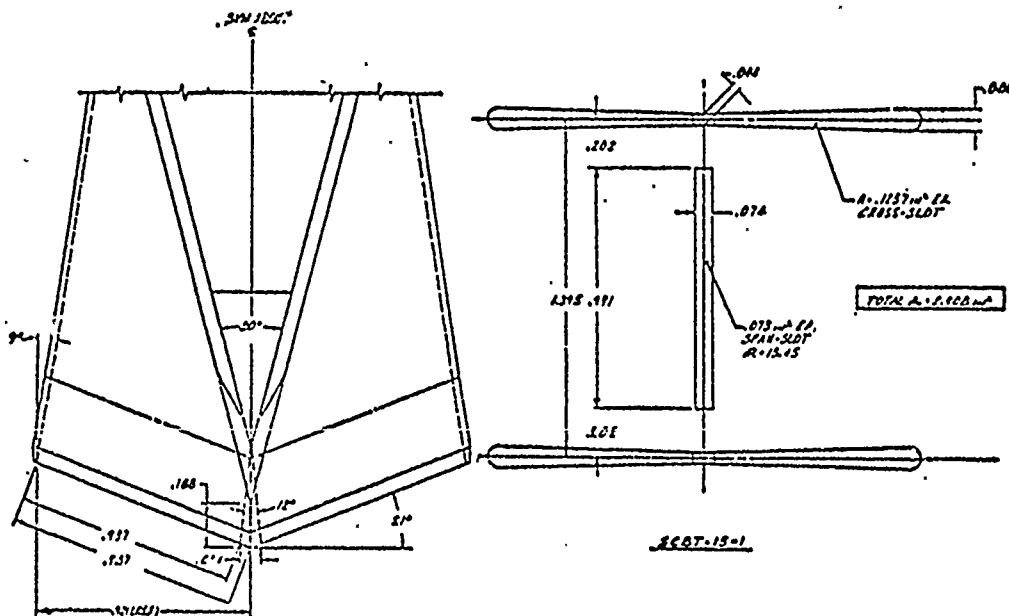
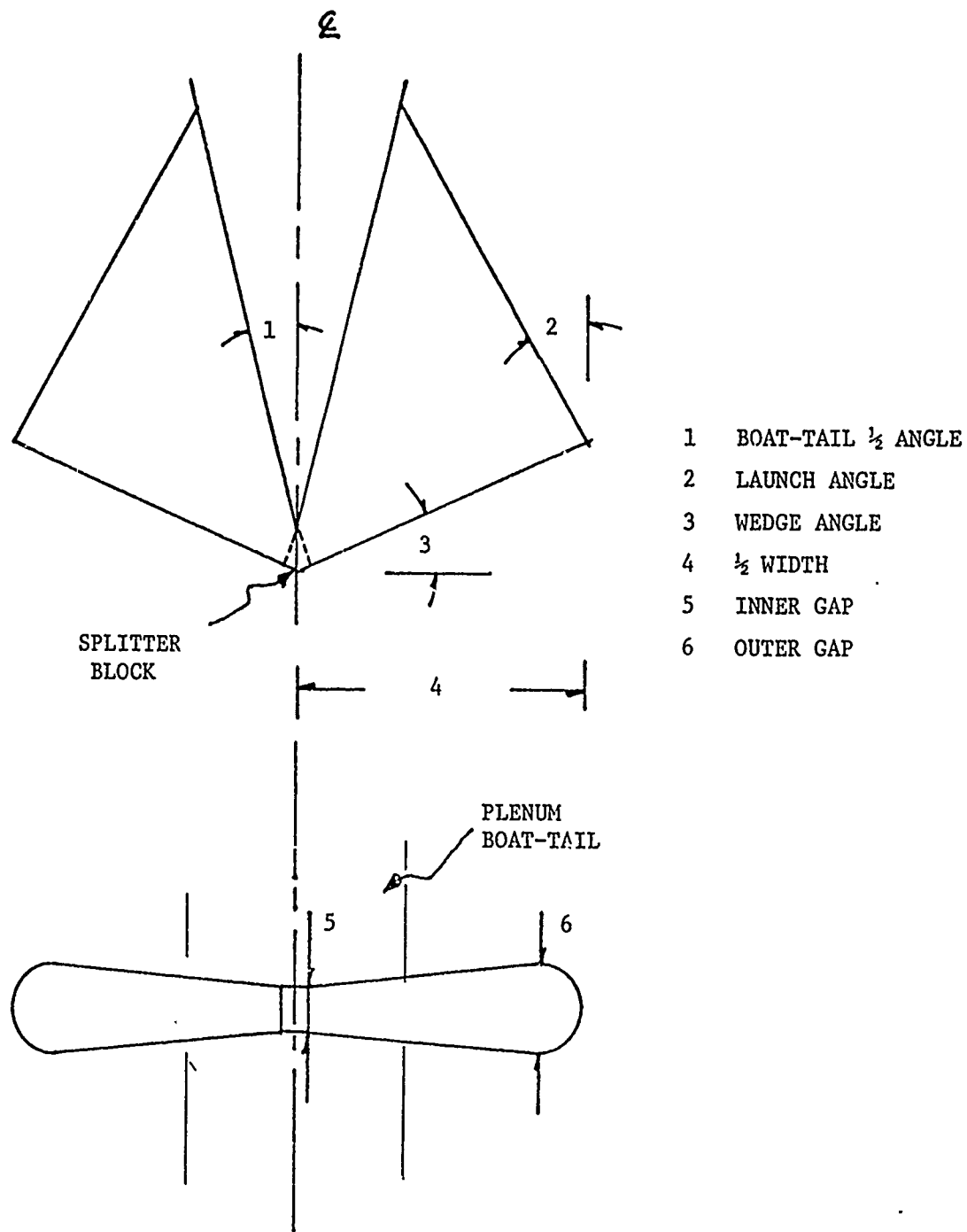


Figure 12. Typical Cross Slot-Span Slot Configuration



BOWTIE RATIO = OUTER GAP/INNER GAP

CROSS SLOT ASPECT RATIO = $(\text{WIDTH} - \text{SPLITTER})^2 / \text{AREA}$

Figure 13. Cross Slot Geometric Parameters

Cross Slot Primary Flow Discharge Angle: Angularity measurements were made. Figure 14 presents the data for four nozzle configurations having the following wedge and launch angles: (a) 0° , 21° ; (b) 21° , 21° ; (c) 11° , 17.2° ; and (d) 21° , 9° . Schematics of the corresponding nozzles are also shown. The abscissa is the nondimensional distance from the centerline to the edge of the nozzle. Measurements were made under four nozzles in each configuration. There is some scatter due to slight manufacturing differences for the small scale model augmenters, evident in Figure 14(c). For analytical purposes, the profile shapes were approximated by straight lines. Calculated $\Delta\phi$'s are shown in Figure 15 for a linearly varying and for a constant angular distribution. The abscissa is the average of the angle at $S = 0$ and $S = 1$. Analytically, a nozzle having the linearly varying flow angle provides a greater $\Delta\phi$. To verify the trend, a cross slot nozzle was designed to provide this type profile (Figure 16). Figure 17 presents a comparison of the measured flow angularity with the desired linear distribution. The results demonstrate that a nozzle can be designed to provide a desired distribution. For this configuration the predicted $\Delta\phi$ was 0.30. The measured value was 0.24 (Figure 15).

Bowtie Ratio: A "bowtie nozzle" shape (cross slot nozzle gap varying, as shown in Figure 12) should increase entrainment and, hence, ϕ by placing more primary flow into the "dog bone" vortices at the cross slot tips (Figure 11). Analytical results are compared with experimental results in Figure 18. Up to a bowtie ratio of about 2, ϕ does increase as predicted.

Span Slot-Cross Slot Flow Split: Both analytical and experimental tests were conducted with the cross slot-span slot configurations to determine the effect of flow split. Flow split is defined as the ratio of the flow through the span slots to the total primary flow. Results are compared with data in Figure 19. Best performance is obtained when the flow to the span slot is about 40 percent or less. These results are understandable since the downstream jet expansion from the span slot can generate destructive interference with the flow from the cross slot.

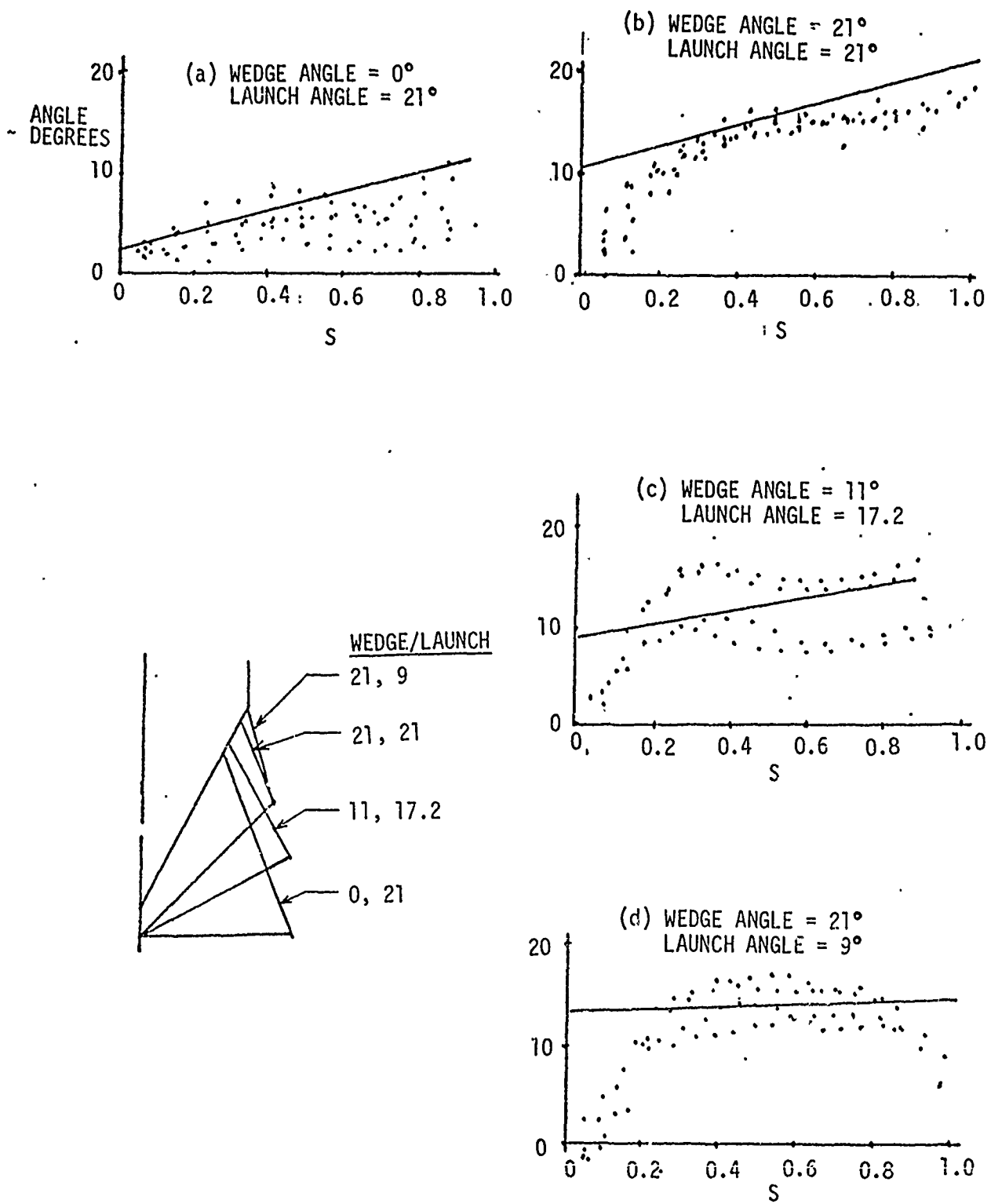


Figure 14. Cross Slot Nozzle Exit Flow Angles

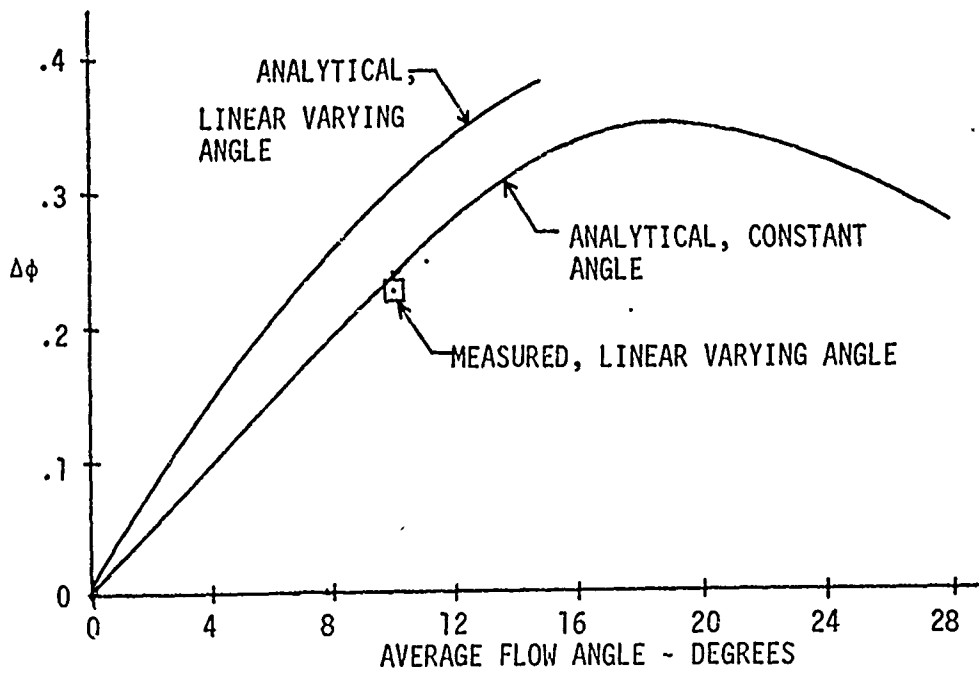


Figure 15. Effect of Constant and Linearly Varying Cross Slot Exit Angularity on $\Delta\phi$.

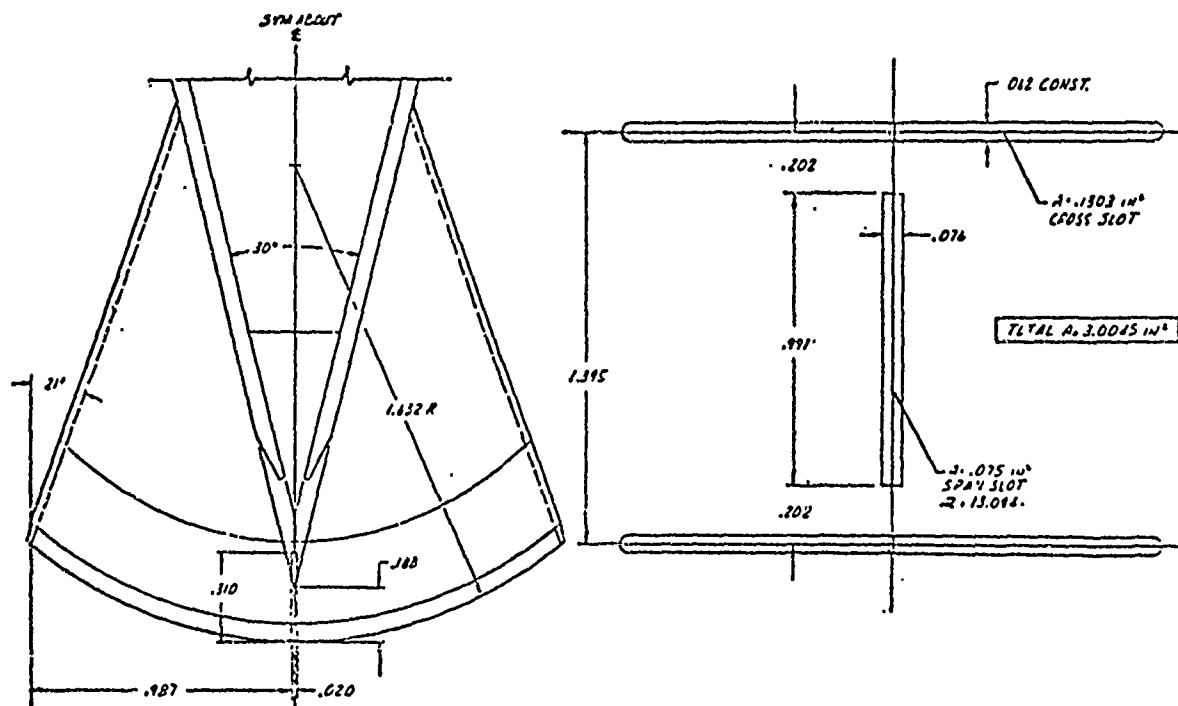


Figure 16. Cross Slot-Span Slot Nozzle with a Linearly Varying Exit Profile.

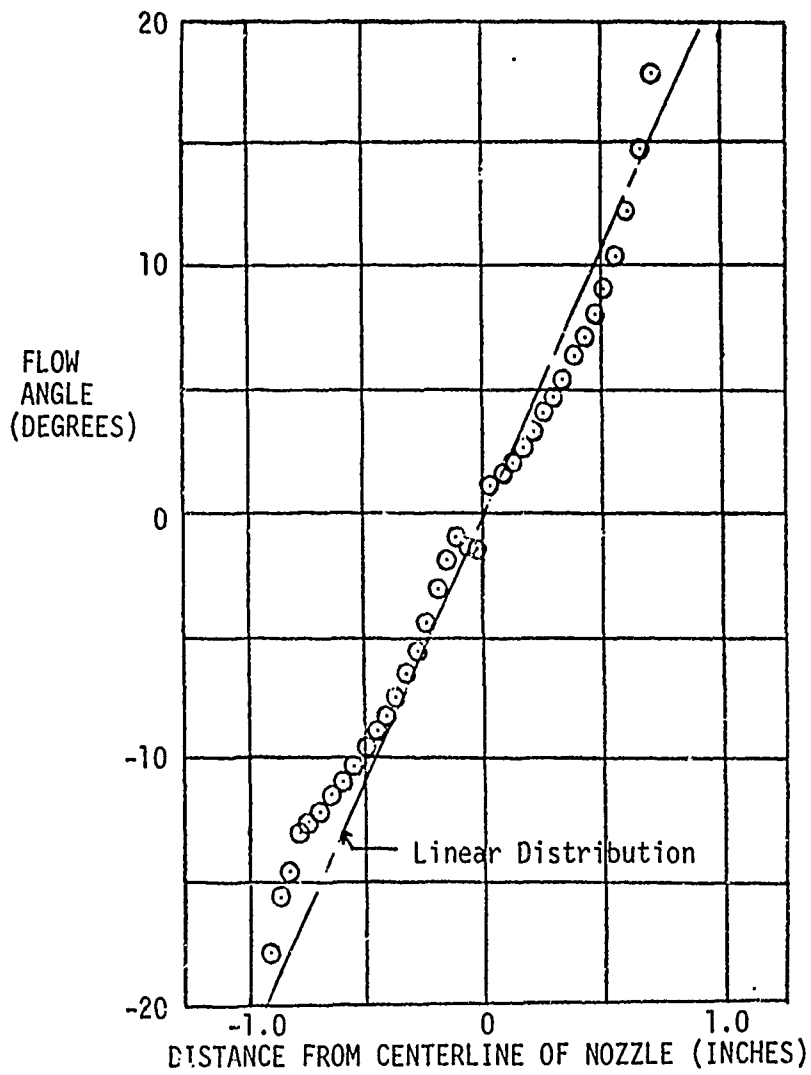


Figure 17. Measured Flow Angles for Linearly Varying Slot Nozzle Configuration.

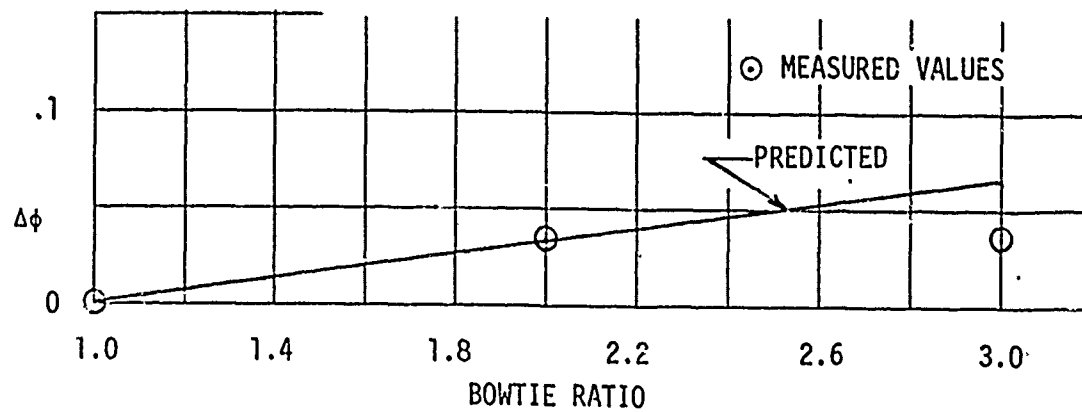


Figure 18. Effect of Bowtie Ratio

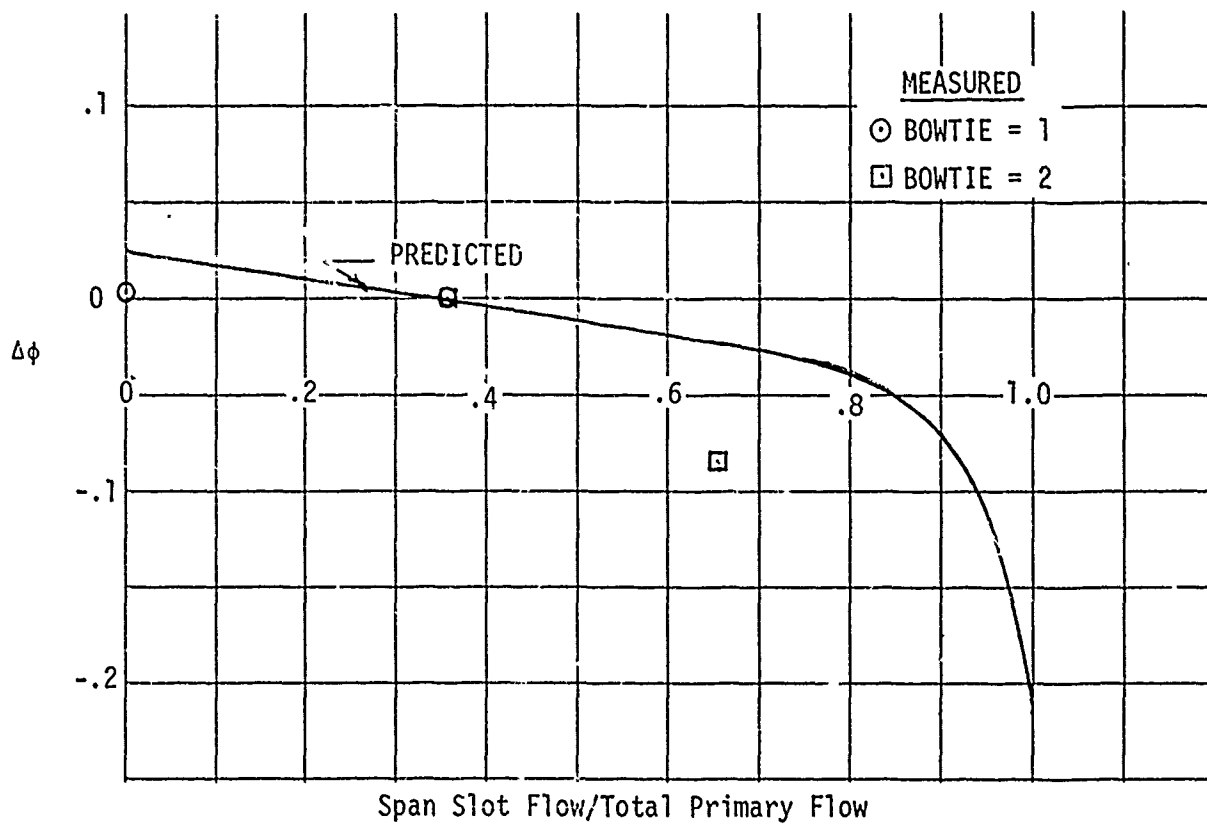


Figure 19. Effect of Flow Split

Cross Slot Aspect Ratio: Since the results in the previous section showed that the percent primary flow to the cross slot nozzle should be increased, the next logical step was to investigate the effect of cross slot aspect ratio. Earlier work by Peschke⁷ showed that the entrainment for 2-dimensional free jets is increased with aspect ratio. Predicted results for augmenters (Figure 20) show that $\Delta\phi$ is increased with cross slot aspect ratio; however, physical width constraints must be considered.

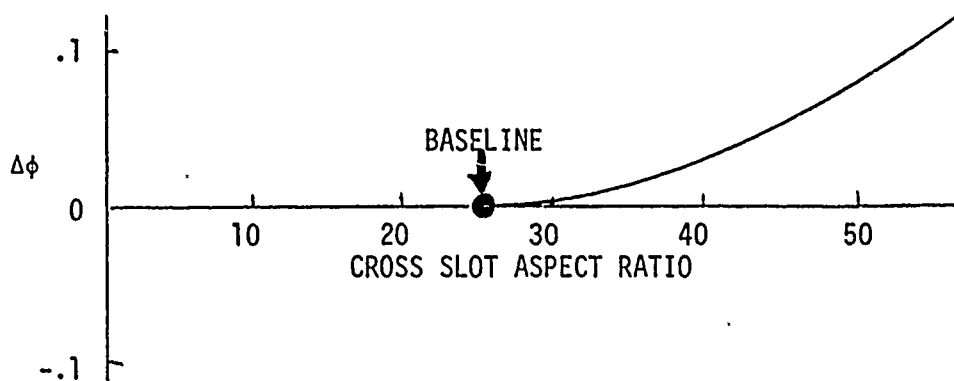


Figure 20. Effect of Cross Slot Aspect Ratio

Symmetric Nozzle Overall Performance: By combining the computer program with tests of the inlet flow angularity, geometric variations, etc., a measured peak ϕ of 1.64 was demonstrated for a cross slot-span slot configuration (Figure 16).

CONCLUSIONS

The following results were obtained from a combined analytical and experimental investigation of centerbody nozzle configurations.

- By combining the data of hypermixing nozzle configurations with a 3-dimensional, turbulent kinetic energy computer program, an analytical procedure was developed for predicting the flow field in ejectors and their augmentation, ϕ .
- The measured ϕ for the 7° hypermixing nozzle, used in the XfV-12A airplane, was 1.45. It was analytically and experimentally shown that a peak ϕ of 1.51 could be obtained by increasing the hypermixing angle to 22°.

- Data for the asymmetric nozzle showed a peak ϕ of 1.55.
- Although larger ϕ 's were obtained by extending the width of the cross slot, optimization studies and tests showed that to increase ϕ it was necessary to increase the bowtie ratio, relative flow to the cross slot, cross slot aspect ratio, and to provide a cross slot, exit velocity angularity which varied linearly with distance.
- By combining the computer program with test data of inlet flow angularity, geometric variations, etc., a measured peak ϕ of 1.64 was demonstrated for the cross slot-span slot configuration in which the exit angularity of the cross slot varied linearly with distance.

REFERENCES

1. Bevilaqua, P. M., Lifting Surface Theory for Thrust-Augmenting Ejectors, AIAA Journal, Vol. 16, No. 5, May 1978, pp. 475-581.
2. Quinn, B. P., Compact Ejector Thrust Augmentation, Journal of Aircraft, Vol. 10, No. 8, August 1973, pp. 481-486.
3. Bevilaqua, P. M., Evaluation of Hypermixing for Thrust Augmenting Ejectors, Journal of Aircraft, Vol. 11, No. 6, June 1974, pp. 348-354.
4. DeJoode, A. D. and Patankar, S. V., Prediction of Three Dimensional Turbulent Mixing in an Ejector, AIAA Journal, Vol. 16, No. 2, February 1978, pp. 145-150.
5. Launder, B. E. and Spalding, D. B., The Numerical Computation of Turbulent Flows, Computer Methods in Applied Mechanics and Engineering, Vol. 3, No. 2, March 1974, pp. 269-289.
6. Mefferd, L. A. and Bevilaqua, P. M., Computer-Aided Design Study of Hypermixing Nozzles, NR78H-91, NASC Contract N00019-77-C-0527, July 1978.
7. Peschke, W., Advanced Ejector Thrust Augmentation Study - Mass Entrainment of Axisymmetric and Rectangular Free Jets, AFFDL-TR-73-55, April 1973.